*Наносистеми, наноматеріали, нанотехнології*
*Nanosistemi, Nanomateriali, Nanotehnologii*
2026, т. 24, № 2, сс. 607–624
https://doi.org/10.15407/nnn.24.02.0607



PACS numbers: 61.05.cp, 68.43.Mn, 81.05.uj, 82.60.Hc, 82.60.Qr, 82.70.Kj, 83.80.Iz

# Thermodynamic Study of the Adsorption of Amaranth Dye on the Surface of a New Activated Nanocarbon Prepared From Petroleum Sources

Muslim Amin Hassan[1], Ahmed Saeed Othman[1], and Ammar Ahmed Hamdoon[2]

[1]*College of Education for Pure Sciences, Department of Chemistry, Tikrit University, Tikrit, Iraq*
[2]*College of Education for Pure Sciences, Department of Chemistry, Mosul University, Mosul, Iraq*

In this study, an activated-nanocarbon model is prepared from petroleum-based sources represented by the Qayyarah asphalt. This asphalt is treated with an aliphatic resin symbolized by $C_5$ in different proportions and in the presence of sulphur. The optimum conditions for the reaction are determined by means of the coefficients using several temperatures, times and sulphur ratios. The study shows that the optimum conditions for the reaction are with the coefficients at 250°C, 2% sulphur, and a time of three hours that is determined by calculating the asphaltenes' ratio. The best model is taken and treated with different distillation processes, both regular and synchronous ones, and then, the distillation-processing waste is taken and treated with potassium hydroxide in proportion of 2.5:1 (raw material:potassium hydroxide) at a temperature of $550 \pm 50$°C for three hours. After that, the resulting nanocarbon material is taken and purified from impurities and base by several processes. The resulting nanocarbon material is taken and its effectiveness is determined by measuring its ability to adsorb the iodine from its aqueous solution, *i.e.*, which is known as the iodine number as a rapid measure of the internal surface area. This research includes the process of removing amaranth dye from its aqueous solution, and the research includes determining the optimal conditions for the adsorption process by studying the factors affecting the adsorption efficiency, which shows that the ideal weight of the prepared activated nanocarbon is of 0.3 g at a concentration of $7 \cdot 10^{-5}$ M and that the reaction equilibrium time is of 70 min. The practical data are applied to models of

different isotherms, such as Langmuir's, Freundlich's, and Temkin's isotherms, at different temperatures for the purpose of using them in calculating the thermodynamic functions. The thermodynamic functions show that the adsorption system is of the physical endothermic type, as indicated by the positive $\Delta H$ values, and that the adsorption process occurs automatically, as indicated by the negative $\Delta G^0$ values, and the adsorption system become more random; due to the ionization of dyes, which are salts of sodium ions, this is indicated by the positive values of $\Delta S^0$.

У цьому дослідженні було виготовлено модель активованого нановуглецю з джерел на основі нафти, представлених асфальтом з Кайяри. Асфальт був оброблений аліфатичною смолою, позначеною як $C_5$, у різних пропорціях й у присутності сірки. Оптимальні умови для реакції було визначено за допомогою коефіцієнтів для кількох температур, часу та пропорцій сірки. Дослідження показало, що оптимальними умовами для реакції є з коефіцієнтами за 250°C, 2% сірки та три години часу. Це було визначено шляхом розрахунку пропорцій асфальтенів. Найліпший модель було обрано й оброблено різними процесами дистиляції, як звичайними, так і синхронними, а потім відходи процесу дистиляції було взято й оброблено гідроксидом Калію у пропорції 2,5:1 (сировина:гідроксид Калію) за температури у $550 \pm 50$°C упродовж трьох годин. Після цього одержаний нановуглецевий матеріял було очищено від домішок та основи за допомогою кількох процесів. Одержаний нановуглецевий матеріял було взято, а його ефективність було визначено шляхом міряння його здатности адсорбувати йод з його водного розчину, тобто так званого йодного числа, яке є оперативним показником площі внутрішньої поверхні. Це дослідження включало процес видалення амарантового барвника з його водного розчину, а також дослідження включало визначення оптимальних умов для процесу адсорбції шляхом вивчення чинників, які впливають на ефективність адсорбції; це показало, що ідеальна вага підготовленого активованого нановуглецю становить 0,3 г за концентрації у $7 \cdot 10^{-5}$ М, а рівноважний час реакції становить 70 хв. Практичні дані було застосовано до моделів різних ізотерм, таких як Ленґмюрові, Фройндлішові та Темкінові ізотерми, за різних температур з метою використання їх для розрахунку термодинамічних функцій. Термодинамічні функції показали, що адсорбційна система є фізичного ендотермічного типу, на що вказують позитивні значення $\Delta H$, і що процес адсорбції відбувається автоматично, на що вказують неґативні значення $\Delta G^0$, причому адсорбційна система стає більш випадковою; через йонізацію барвників, які є солями йонів Натрію, це було продемонстровано позитивними значеннями $\Delta S^0$.

**Key words:** activated nanocarbon, aliphatic resin, Qayyarah asphalt, amaranth pigment, thermodynamic functions.

**Ключові слова:** активований нановуглець, аліфатична смола, асфальт Кайяри, амарантовий піґмент, термодинамічні функції.

*(Received 23 January, 2025)*

## 1. INTRODUCTION

Water pollution has become a global problem now, and there is a constant need for water resources policy assessment to address this problem; water pollution causes the death of 14 000 people every day in the world, and the problem of water pollution faces both developed and developing countries, as water quality is affected by many factors, such as rainfall, climate, soil type, vegetation, geology, soil conditions, groundwater, and human activities [1].

Activated nanocarbon refers to a wide range of nanocarbonized materials with a high degree of porosity and high surface area. Activated nanocarbon has many applications in the environment and industry in the field of removing, recovering, separating, and modifying various compounds in the liquid and gaseous phases. Activated nanocarbon prepared using potassium hydroxide has a high surface area and better efficiency than sodium hydroxide in various applications [2].

The use of nanocarbon dates back to 3750 B.C. to reduce copper (Cu), zinc (Zn), and tin (Sn) ores in the manufacture of bronze by the Egyptians and Sumerians. In 157 A.D., plant and animal-based nanocarbons were used to treat a wide range of diseases [3].

Liang and his colleagues a series of activated nanocarbon models from asphalt for adsorption of ethane and ethylene. The results showed that the models prepared at 800°C and KOH:asphalt ratio = 4 showed a high surface area through BET measurements. It amounted to 3111 $m^2/g$ and its pore volume was of 1.92 $cm^2/g$. The prepared activated nanocarbon showed higher adsorption of $C_2H_6$ over $C_2H_4$ [4].

Javed and his group were able to synthesize a porous activated nanocarbon with a high surface area derived from low-cost asphalt (AS) and study its efficiency in adsorption of bisphenol A (BPA), a common endocrine disrupting chemical (EDC) in wastewater and natural water. The results generally showed that AS is a highly efficient adsorbent for removing EDC for water purification and can be adopted in drinking water treatment and wastewater polishing [5].

Han *et al.* prepared an effective nanocarbon-based adsorbent using asphaltenes from asphalt rocks. They took asphaltenes from natural asphalt rocks in Indonesia as raw materials to prepare a microporous nanocarbon material through pyrolysis < 500°C and potassium-hydroxide activation processes. The optimum activation conditions were obtained at a potassium hydroxide:charcoal ratio of 3:1 and 800°C for 30 min. Additional adsorption tests indicated that the adsorption of methylene blue on the porous nanocarbon material is monolayer adsorption. The maximum adsorption capaci-

ty was determined at 556 mg/g, which is much higher than some commercial activated nanocarbons. It is also noted that the adsorption kinetics follow the pseudo-second-order model. These results indicate that asphaltenes-derived nanocarbons will be promising and effective adsorbents [6].

Wang *et al.* prepared magnetic asphalt-based activated nanocarbon in one-step with high specific surface area and adsorption performance of methylene blue. The results showed that the nanocarbon had a micromedium porous structure, the adsorption reaction results were endothermic and spontaneous, the Langmuir's isotherm model was applied to it, and the reaction order was pseudo-second order [7].

Gorbunova *et al.* chose a simple method to predict and guide the porous structure of activated nanocarbon derived from petroleum asphalt.

In the present work, the correlation between the structural and adsorption properties of asphalt-based porous nanocarbon and the nanocarbonization temperature was found. In addition, the optimum nanocarbonization temperature was determined, and the reasons for the effect of nanocarbonization temperature on the main structural properties of activated nanocarbon were investigated. Nanocarbonization temperature of 500–600°C for petroleum asphalt was found to be optimal for further activation. Potassium-hydroxide activation of nanocarbonized petroleum asphalt at 500–600°C provides small porous nanocarbon with high surface area [8].

The presence of dyes in water has unusual effects on human life, given the large global consumption of dyes from the food, cosmetics, textile and pharmaceutical sectors, which reaches 1.000.000 tons worldwide. The complex structures of dyes consisting of aromatic rings linked to different functional groups with a $\pi$-electron can absorb light in the spectral range of 380–700 nm [9].

Toxic wastes containing azo dyes are discharged from various industries, negatively affecting water resources, soil fertility, aquatic organisms and the health of the ecosystem. It has toxic and lethal effects, causes mutations and cancer in aquatic organisms and animals, is not easily biodegradable under natural conditions and is not usually removed from wastewater by conventional wastewater treatment systems. Benzidine-based dyes have long been recognized as carcinogenic to the human bladder and tumorigenic [10].

**Amaranth Dye.** Amaranth dye has been evaluated several times by the Joint FAO/WHO Expert Committee on Food Additives in 1972, 1975, 1978 and 1984 and by the Scientific Committee on Food of the European Union (SCF) in 1976, 1979 and 1983.

Studies in rodents indicate that amaranth is poorly absorbed (2.8% in rats) after oral administration; therefore, the majority

**TABLE 1.** Amaranth and its chemical composition.

| Name | Structure | $M$, g·mol$^{-1}$ | Melting point, °C | $\lambda_{max}$, nm | Colour |
|---|---|---|---|---|---|
| Sodium 7-hydroxy-8-((4-sulfonatonaphthalen-1-yl)diazenyl)naphthalene-1,3-disulfonate (E 123) | 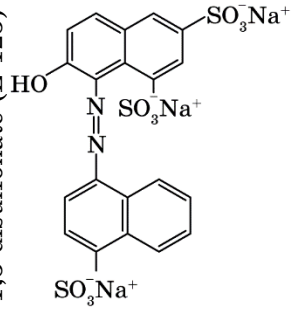 | 604.47 | 120 | 524 | red |

remains in the intestinal content [11, 12].

## 2. PRACTICAL PART

**First: Treatment of Qayyarah Asphalt with Additives.** A known weight of Qayyarah asphalt was taken and treated with different proportions of $C_5$ resin in the presence of sulphur at a temperature range between 200–300°C, as the optimal conditions for the treatment process were determined.

**Second: Separation of Asphaltenes.** One gram of the original asphalt, modified asphalt and the treated asphalt was taken and dissolved in 40 ml of petroleum ether at 60–80°C and the mixture was shaken for three hours in an ice bath; then, the sample was filtered and washed with distilled water several times until the result of the washing process became colourless. The asphaltenes were dried and weighed, and then, their percentage was calculated.

**Third: Preparation of the Raw Material for the Preparation of Activated Nanocarbon.** A very good sample obtained in terms of asphaltenes' content was taken, and regular and vacuum distillation processes were carried out on it in order to increase the nanocarbon mass of the raw material.

**Fourth: Preparation of Activated Nanocarbon.** The material resulting from step (second) was taken and treated with potassium hydroxide at a ratio of 1:2.5 (waste:potassium hydroxide) at a temperature degree of 550–600°C for three hours.

The nanocarbon material was then cooled and washed with distilled water several times until neutralization, then treated with a 5% hydrochloric acid solution by thermal sublimation for two

hours. The nanocarbon material was cooled, then filtered and washed with distilled water several times until neutralization, then dried and stored with a particle size of 150 μm, thus, making it ready to measure its effectiveness.

**Fifth: Determining the Effectiveness of Activated Nanocarbon. *A*: Iodine Adsorption from Its Aqueous Solution.** One gram of the prepared activated nanocarbon was taken and placed in a conical flask with a capacity of 250 ml, and 100 ml of iodine solution with a concentration of 0.1 N was added. The mixture was shaken for half an hour, and then, the dye solution was separated by filtration, taking care to neglect 20 ml of the solution at the beginning of the filtration to avoid the effect of the adsorption of the filter paper on the dye solution as well as the calibration process.

To complete the measurement, 50 ml of iodine solution was taken and titrated with sodium thiosulphate aqueous at a concentration of 0.1 N, using starch as a reagent medium, where the volume of thiosulphate used was calculated for the purpose of calculating the iodide adsorbed by the prepared activated nanocarbon, according to the relationships:

$$X = A - 2.2B \text{ [ml of thiosulphate used]}, \tag{1}$$

$$A = 12693N_1, \tag{2}$$

$$B = 126.93N_2; \tag{3}$$

$X$ is weight of iodine adsorbed [in mg] by the activated nanocarbon, $N_1$ and $N_2$ are standard of iodine solution and standard of sodium thiosulphate, respectively (0.1 N).

The iodine number [13] is calculated through the equation

$$I.N. = X/\mathrm{M}D, \tag{4}$$

where $X$ is weight of nanocarbon used, $D$ is correction factor.

**Making a Calibration Curve and Finding the Wavelength of Maximum Absorption. *B*: Amaranth Dye Adsorption.** For determining the wavelength of maximum absorption of the dye, multiple concentrations ($1{\cdot}10^{-5}$–$9{\cdot}10^{-9}$ M) of amaranth solution were prepared to be used, when measuring concentrations before and after the adsorption process.

A relationship was drawn between absorption and concentration to obtain a main equation, through which the unknowns were calculated and based on the Beer–Lambert law:

$$A = \varepsilon LC; \tag{5}$$

$A$ represents the dye absorption, ε is the molar absorption coeffi-

cient ($l \cdot mol^{-1} \cdot cm^{-1}$), $L$ is the optical-path length of visible rays ($L = 1$ cm), and $C$ the molar concentration ($mol \cdot l^{-1}$) [13].

**Effect of the Amount of Adsorbent.** The effect of the amount of adsorbent on the adsorption efficiency was studied, using the dye solution at a concentration of $7 \cdot 10^{-5}$ M with changing the amount of adsorbent in a range between 0.05–0.3 g, at a temperature of 25°C, and a volume of 10 ml.

**Determining the Equilibrium Time.** In order to monitor the adsorption of the dye under study, a kinetic study was conducted to determine the time required for the adsorption system to reach equilibrium, by measuring the absorbance at a time of 10, 20, 30, 40, 50, 60, 70, 80, 90 minutes.

**Calculating Thermodynamic Functions.** The enthalpy values of adsorption $\Delta H$ can be calculated by calculating the value of the equilibrium constant at different temperatures [14]:

$$\ln K = \text{const} - \Delta H/(RT). \tag{6}$$

The value of the equilibrium constant can be calculated through the equation

$$K = C_{ad}/C_e. \tag{7}$$

The value of $\Delta H$ was calculated by drawing a relationship between $\ln K$ *versus* $1/T$ to give a straight line with a slope equal to $-\Delta H/R$ [15] (here, $R$ represents the gas constant of 8.314 $J \cdot mol^{-1} \cdot k^{-1}$), while the values of $\Delta G^0$ and $\Delta S^0$ were calculated based on the following equations:

$$\Delta G^0 = -RT \ln K, \tag{8}$$

$$\Delta S^0 = (\Delta H^0 - \Delta G^0)/T. \tag{9}$$

## 3. APPLICATION OF ADSORPTION ISOTHERMS

**First: Langmuir's Isotherm.** When drawing a relationship between $C_e/q_e$ *versus* $C_e$, that gives a slope of $1/q_{\max}$ and a section of $1/(bq_{\max})$ [16], at different temperatures:

$$\frac{C_e}{q_e} = \frac{1}{bq_{\max}} + \frac{C_e}{q_{\max}}. \tag{10}$$

**Second: Freundlich's Isotherm.** The Freundlich's isotherm equation was applied at temperatures ranging between 328–288 K, and the values of Freundlich's constants ($K$, $n$) were calculated from the slope ($1/n$) [17], and the straight-line segment ($\log K$) resulting from

drawing the relationship between $\log q_e$ *versus* $\log C_e$:

$$\log q_e = \log K + n^{-1} \log C_e . \quad (11)$$

**Third: Temkin's Isotherm.** Drawing the relationship between $q_e$ *versus* $\ln C_e$, at different temperatures, that gives the slope value of the straight line that equals to $B_T$ [18], and a segment equal to $K_T$:

$$q_e = B_T \ln K_T + B_T \ln C_e . \quad (12)$$

## 4. RESULTS AND DISCUSSION

**Asphalt Treatment with Additives.** Qayyarah asphalt was treated with the additives used in this study, as shown in the first paragraph of the Practical Part and Tables 2–4; it is shown the percentages of asphaltenes separated from the original asphalt and the

**TABLE 2.** Percentages of asphaltenes separated at 250°C and at different times and with 2% by weight of sulphur.

| Samples | Time, hr | Asphaltenes, % |
|---|---|---|
| $AS_0$ | — | 43 |
| $AS_1$ | 2 | 52 |
| $AS_2$ | 3 | 72 |
| $AS_3$ | 4 | 60 |
| $AS_4$ | 5 | 54 |

**TABLE 3.** Percentages of asphaltenes separated, using different sulphur ratios at 250°C.

| Samples | S, % | Asphaltenes, % |
|---|---|---|
| $AS_5$ | 1 | 50 |
| $AS_6$ | 2 | 72 |
| $AS_7$ | 3 | 66 |

**TABLE 4.** Percentages of asphaltenes separated, using 2% sulphur, at different temperatures and time of 3 hours.

| Sample | $T$, °C | Asphaltenes, % |
|---|---|---|
| $AS_8$ | 200 | 39 |
| $AS_9$ | 250 | 72 |
| $AS_{10}$ | 300 | 51 |

treatment at different reaction conditions for determining the optimum conditions for this treatment.

**$AS_0$: Original Model.** The results in Tables 2–4 showed that the best model for preparing activated nanocarbon is to use 2% sulphur, 10% $C_5$, with a heating time of 3 hours at a temperature of 250°C. This was clear from the asphaltenes' ratio that was obtained, which reached 72%, and then preparing activated nanocarbon by choosing the best model.

Activated nanocarbon was prepared from the best model in terms of asphaltenes' content that was obtained through the aforementioned processing, as explained in fourth paragraph of the Practical Part. The properties of the prepared activated nanocarbon were determined, as its effectiveness was determined by the adsorption of iodine dye from its aqueous solution, as the model gave an excellent iodine-number value of 1129.677 mg/g.

Iodine number is considered as a measure of the internal surface area of activated nanocarbon [19]. In order to determine the effectiveness of activated nanocarbon in the adsorption of dyes with a large structural formula, the effectiveness of nanocarbon was measured through the adsorption of amaranth dye, as shown in the fifth paragraph and its branches. In order to cover all matters related to the prepared activated nanocarbon, the infrared spectrum, scanning electron microscopy (SEM) [20], energy dispersion of x-rays (EDX) and x-ray diffraction (XRD) were measured.

The EDX results gave the following Fig. 1. The values obtained through measuring EDX (energy dispersion of x-rays) [21] indicated that the nanocarbon ratio is very high compared to other elements that may have appeared as a result of measurement or work conditions.

XRD measurements indicated that the prepared sample is non-crystalline [22], and this was clearly shown through the wide band

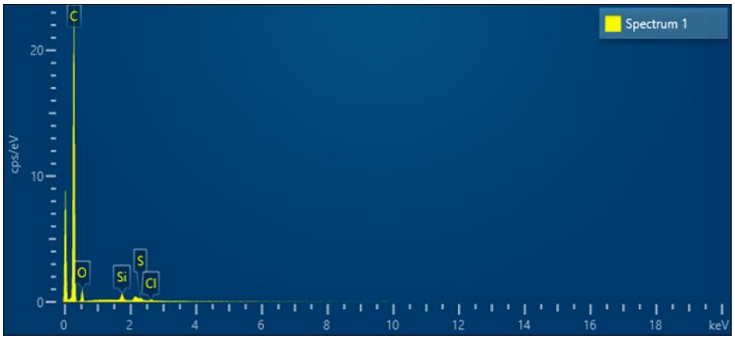


**Fig. 1.** Elemental ratios in activated nanocarbon.

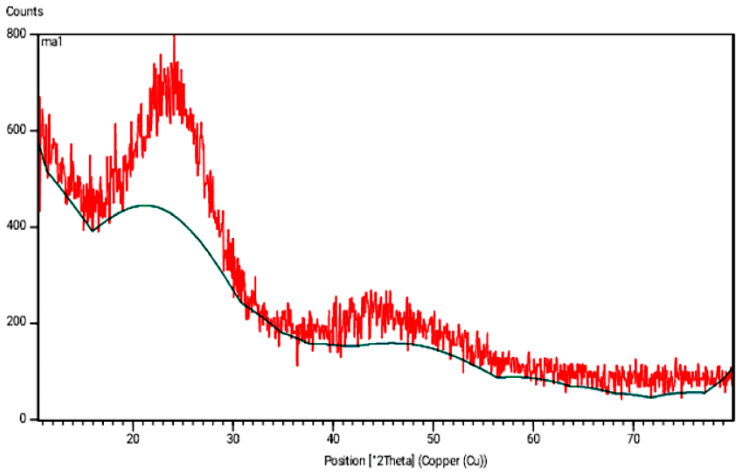


**Fig. 2.** X-ray diffraction of activated nanocarbon.

**TABLE 5.** Results of adsorption measurements using the BET method.

| Measurement | Analysis data |
|---|---|
| Surface area | 764.62 $m^2/g$ |
| Pore volume | 0.4277 $cm^3/g$ |
| Average pore diameter | 2.2372 nm |

2-Theta that is ranged between 20 and 30.

The results of the adsorption measurements using the BET method showed that the prepared activated nanocarbon has a large surface area, small grain size, and small average pore size [23], as shown in Table 5.

The process of preparing activated nanocarbon using hydroxides is one of the most important preparation methods, as it is a nanocarbonization and activation process at the same time, as the hydroxide ions present in potassium hydroxide work to withdraw hydrogen from the raw material in the form of $H_2O$, leaving the positive ion to control the size and type of pores formed in the activated nanocarbon, as it was found that the radius of the positive ion is the controller of the size, type and efficiency of the pores formed in the activated nanocarbon [24].

## 5. STUDIES' RESULTS

**Making a Calibration Curve and Finding the Wavelength of Maximum Absorption.** After measuring the absorbance of the dye at concentrations of $1{\cdot}10^{-5}$–$9{\cdot}10^{-9}$ M, it was found that the dye was

subject to the Beer–Lambert law and obtained a high correlation coefficient.

**Effect of the Amount of Adsorbent.** After studying the effect of the amount of adsorbent, the following results were obtained.

The adsorption-efficiency values showed that the preferred weight for adsorption of activated nanocarbon is of 0.3 g, which

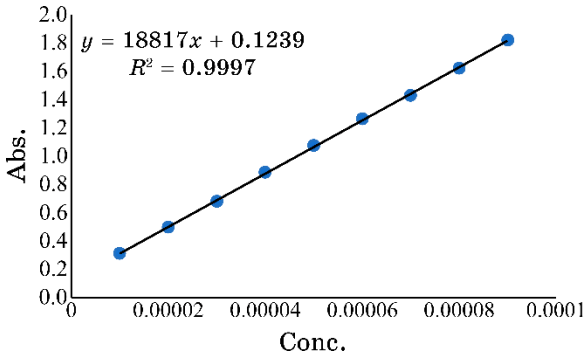


**Fig. 3.** Calibration curve for amaranth dye.

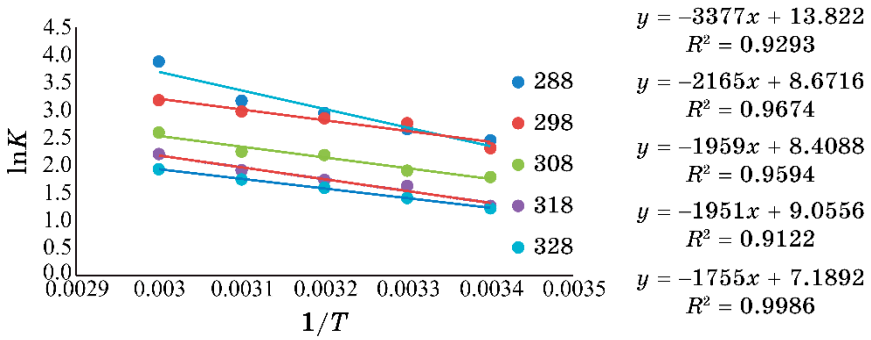


**Fig. 4.** The relationship between ln$K$ *vs.* $1/T$ to calculate the values of adsorption enthalpy.

**TABLE 6.** Effect of the amount of activated nanocarbon on the adsorption efficiency at a temperature of 25°C and a concentration of $7 \cdot 10^{-5}$ M.

| Weight, g | $C_e$, mg/l | $q_e$, mg/g | Efficiency, % |
|---|---|---|---|
| 0.05 | 22.297 | 4.003 | 47.31 |
| 0.1 | 6.332 | 3.598 | 85.03 |
| 0.15 | 4.436 | 2.525 | 89.52 |
| 0.2 | 2.091 | 2.011 | 95.06 |
| 0.3 | 0.421 | 1.396 | 98.96 |

**TABLE 7.** Effect of reaction time on adsorption efficiency.

| Time, min | $C_e$, mg/l | $q_e$, mg/g | Efficiency, % |
|---|---|---|---|
| 10 | 6.813 | 2.357 | 83.90 |
| 20 | 6.139 | 2.412 | 85.49 |
| 30 | 5.914 | 2.427 | 86.02 |
| 40 | 5.496 | 2.454 | 87.01 |
| 50 | 4.886 | 2.495 | 88.45 |
| 60 | 4.565 | 2.517 | 89.21 |
| 70 | 3.826 | 2.566 | 90.95 |
| 80 | 7.938 | 2.292 | 81.24 |
| 90 | 9.962 | 2.157 | 76.46 |

means that increasing the amount of the adsorbent leads to an increase in the number of sites eligible for adsorption, and this increase raises the efficiency of the adsorbent in removing the dye from the aqueous solution. 0.15 g of activated nanocarbon was chosen for conducting subsequent studies within this study. Because this represents a middle ground and because large amounts lead to complete removal of the adsorbent, it is difficult to study it [25].

**Determining the Equilibrium Time.** By measuring the absorbance at different times, using 10 ml of the dye solution and a concentration of $7 \cdot 10^{-5}$ M at a temperature of 25°C, the results were obtained, as shown in Table 7.

During the reaction, we noticed that adsorption occurred at a high rate in the first ten minutes of the reaction, after which the adsorption process began to slow down gradually until it reached equilibrium at 70 min, according to the availability of a large number of empty active sites on the surface of the adsorbent, which are qualified to bind to the dye that decreases gradually with time [26].

## 6. CALCULATING THE THERMODYNAMIC FUNCTIONS

$\Delta H$ was calculated by drawing a relationship between $\ln K$ *versus* $1/T$ to give a straight line with a slope equal to $-\Delta H/R$ (here, $R$ represents the gas constant of 8.314 $J \cdot mol^{-1} \cdot K^{-1}$) as in Eq. (6), while the values of $\Delta G^0$ and $\Delta S^0$ were calculated based on Eq. (8), (9).

It was noted from the results listed in Table 8 that the values of the equilibrium constant $K$ increase with increasing temperature at a constant concentration, as well as increasing the adsorption capacity with increasing temperature.

The positive sign of the adsorption-heat values ($\Delta H$) indicates that the nature of the association is endothermic [27] between the

**TABLE 8.** Values of equilibrium constants and thermodynamic functions at different concentrations and different temperatures.

| Concentration, M | $T$, K | $K$ | $\Delta H$, kJ·mol$^{-1}$ | $\Delta S^0$, J·mol$^{-1}$·K$^{-1}$ | $\Delta G^0$, kJ·mol$^{-1}$ |
|---|---|---|---|---|---|
| | 288 | 11.531 | | 117.813 | –5.854 |
| | 298 | 14.150 | | 116.248 | –6.566 |
| $5\cdot10^{-5}$ | 308 | 18.976 | 28.076 | 115.623 | –7.536 |
| | 318 | 23.693 | | 114.604 | –8.368 |
| | 328 | 48.225 | | 117.823 | –10.570 |
| | 288 | 10.057 | | 75.510 | –5.526 |
| | 298 | 15.822 | | 77.389 | –6.841 |
| $6\cdot10^{-5}$ | 308 | 17.179 | 16.221 | 76.312 | –7.283 |
| | 318 | 19.490 | | 75.701 | -7.852 |
| | 328 | 24.030 | | 75.887 | –8.670 |
| | 288 | 5.929 | | 71.351 | –4.262 |
| | 298 | 6.699 | | 70.466 | –4.712 |
| $7\cdot10^{-5}$ | 308 | 8.895 | 16.287 | 71.045 | –5.595 |
| | 318 | 9.445 | | 69.881 | –5.935 |
| | 328 | 13.300 | | 71.171 | –7.057 |
| | 288 | 3.519 | | 72.958 | –3.012 |
| | 298 | 5.068 | | 73.896 | –4.021 |
| $8\cdot10^{-5}$ | 308 | 5.658 | 18.000 | 72.851 | –4.438 |
| | 318 | 6.716 | | 72.434 | –5.034 |
| | 328 | 9.029 | | 73.168 | –5.999 |
| | 288 | 3.375 | | 60.774 | –2.912 |
| | 298 | 4.069 | | 60.628 | –3.476 |
| $9\cdot10^{-5}$ | 308 | 4.878 | 14.591 | 60.552 | –4.059 |
| | 318 | 5.665 | | 60.299 | –4.584 |
| | 328 | 6.873 | | 60.515 | –5.258 |

dye molecules and the surface of the activated nanocarbon. The results show that the values of $\Delta H$ are less than 40 kJ·mol$^{-1}$ that proves that the adsorption is of a physical nature [28].

The positive values of $\Delta S^0$ showed an increase in the randomness of the studied system [29], and this may be due to the nature of the dye used, which is sodium salt that is ionized in the aqueous solution, releasing sodium ions that causes an increase in the randomness of the system.

Negative values of $\Delta G^0$ indicate that the adsorption process is spontaneous, and that the spontaneity of the reaction increases with increasing temperature, due to the reaction being endothermic inside the solution [30].

## 7. APPLICATION OF ADSORPTION ISOTHERMS

**First: Langmuir's Isotherm.** When drawing the relationship between $C_e/q_e$ *versus* $C_e$, which gives a slope of $1/q_{max}$ and a section of $1/(bq_{max})$, at different temperatures [31], the results obtained are listed in Table 9.

The results of the Langmuir's isotherm showed a good direct relationship with the increase in temperature. This indicates the applicability of this model to the adsorption process. We also note the increase in the constant $b$ [32]. The values of $q_{max}$ and $b$ of the Langmuir's isotherm at different concentrations and different temperatures are listed in Table 9.

**Second: Freundlich's Isotherm.** The values of Freundlich's constants ($K$, $n$) were calculated from the slope $1/n$ and the straight-line segment log$K$, resulting from drawing the relationship between log$q_e$ *versus* log$C_e$, and these values are listed in Table 10.

The values of Freundlich's constants gave good linear relation-

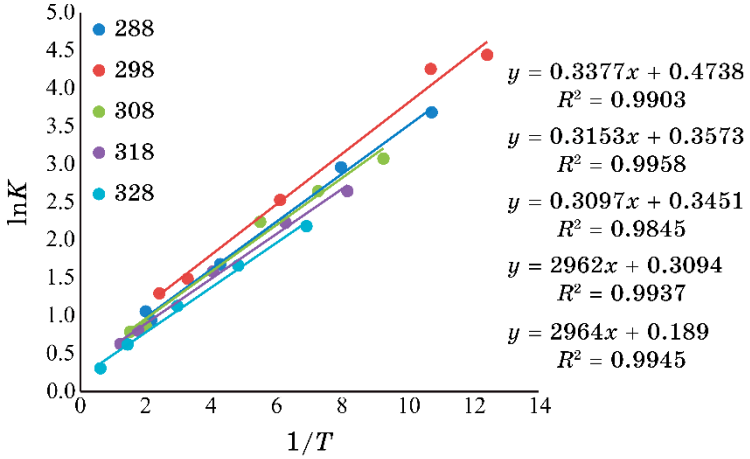


**Fig. 5.** The relationship between $C_e/q_e$ *vs.* $C_e$ for the Langmuir's isotherm.

**TABLE 9.** Values of the Langmuir's constants and correlation coefficients ($R$) obtained from the Langmuir's isotherm.

| $T$, K | $b$, l/mg | $q_{max}$, mg/g | $R$ |
|---|---|---|---|
| 288 | 0.704 | 2.997 | 0.9951 |
| 298 | 0.882 | 3.172 | 0.9979 |
| 308 | 0.897 | 3.229 | 0.9922 |
| 318 | 0.957 | 3.376 | 0.9968 |
| 328 | 1.568 | 3.374 | 0.9972 |

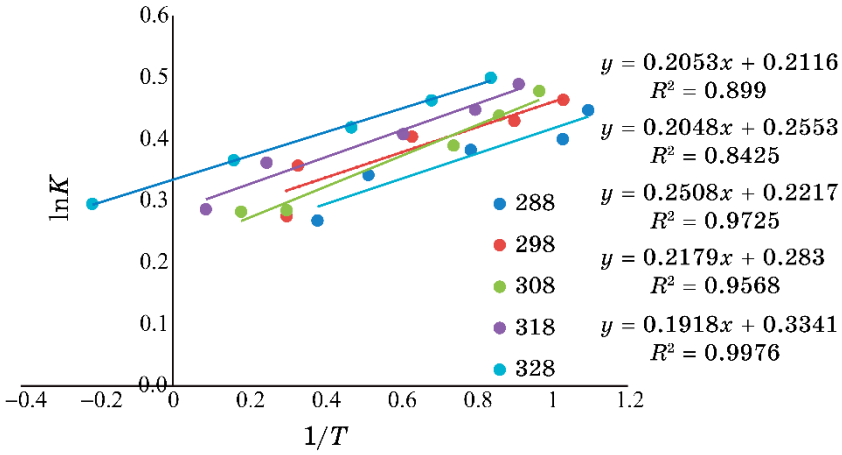


**Fig. 6.** The relationship between $\log C_e$ *vs.* $\log q_e$ for the Freundlich's isotherm.

**TABLE 10.** Values of Freundlich's constants and correlation coefficients ($R$) obtained when applying the Freundlich's isotherm.

| $T$, K | $n$ | $K$ | $R$ |
|---|---|---|---|
| 288 | 4.871 | 1.628 | 0.9486 |
| 298 | 4.883 | 1.800 | 0.9179 |
| 308 | 3.987 | 1.667 | 0.9862 |
| 318 | 4.589 | 1.919 | 0.9782 |
| 328 | 5.214 | 2.158 | 0.9988 |

ships at different temperatures [33], and the values of $n$ indicated that the adsorption is of the preferred type.

**Thirdly: Temkin's Isotherm.** When drawing the relationship between $q_e$ *versus* $\ln C_e$ at different temperatures, from the value of the slope of the straight line that is equal to $B_T$ and with an intercept equal to $K_T$, the curves in Fig. 7 and the values fixed in Table 11 were obtained. The values of the correlation coefficient $R$ indicate good linear relationships at different temperatures, which indicate the possibility of applying this isotherm to such types of systems. In addition, the increase in the values of the constant $K_T$ with increasing temperature is consistent with the positive sign of the enthalpy.

## 8. CONCLUSIONS

The process of extracting amaranth dye from its aqueous solution

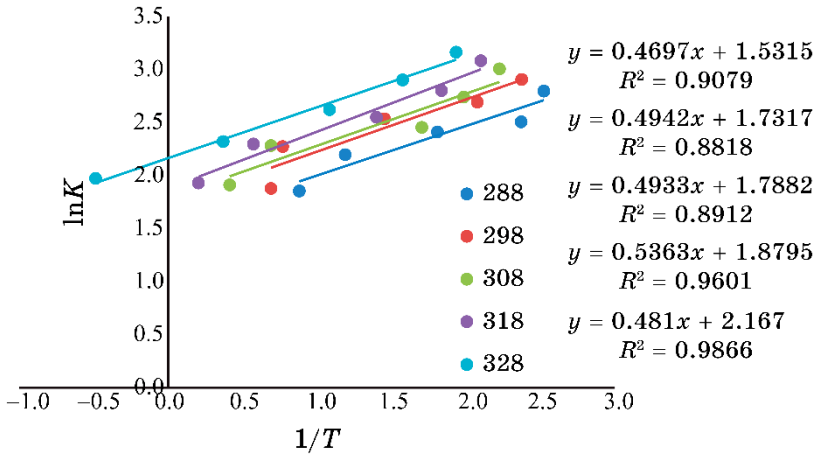


**Fig. 7.** The relationship between $q_e$ *vs.* $\ln C_e$ for the Temkin's isotherm.

**TABLE 11.** Values of the Temkin's constants and the correlation coefficients ($R$) obtained when applying the Temkin's isotherm.

| $T$, K | $B_T$ | $K_T$, l/mg | $R$ |
|---|---|---|---|
| 288 | 0.4697 | 1.5315 | 0.9528 |
| 298 | 0.4942 | 1.7317 | 0.9390 |
| 308 | 0.4933 | 1.7882 | 0.9440 |
| 318 | 0.5363 | 1.8795 | 0.9798 |
| 328 | 0.481 | 2.167 | 0.9933 |

was part of this study, which also looked at the factors, which affect adsorption efficiency.

The results show that the ideal weight of the prepared activated nanocarbon is of 0.3 g at a concentration of $7 \cdot 10^{-5}$ M; the equilibrium reaction time is of 70 min. The practical data are applied to models of different isotherms, such as Langmuir's, Freundlich's, and Temkin's isotherms, at different temperatures for using them in calculating the thermodynamic functions. Thermodynamic functions show that the adsorption system is of the physical endothermic type, as indicated by the positive $\Delta H$ values; the adsorption process occurs automatically. The adsorption system grew more random, as shown by the negative $\Delta G^0$ values; the positive $\Delta S^0$ data show that dyes, which are salts of Na ions, are ionized.

## REFERENCES

1. F. N. Chaudhry and Mohammad Fawad Malik, *J. Ecosyst. Ecography*, **7**,

No. 1: 225 (2017); doi:10.4172/2157-7625.1000225
2. P. González-García, *Renewable and Sustainable Energy Reviews*, **82**: 1393 (2018); https://doi.org/10.1016/j.rser.2017.04.117
3. T. Gupta and T. Gupta, *Carbon: the Black, the Gray and the Transparent*, **47**: 70 (2018); https://doi.org/10.1007/978-3-319-66405-7_2
4. W. Liang, Y. Zhang, X. Wang, Y. Wu, X. Zhou, J. Xiao, and Z. Li, *Chemical Engineering Science*, **162**: 192 (2017); https://doi.org/10.1016/j.ces.2017.01.003
5. H. Javed, D. X. Luong, C. G. Lee, D. Zhang, J. M. Tour, and P. J. Alvarez, *Carbon*, **140**: 441 (2018); https://doi.org/10.1016/j.carbon.2018.08.038
6. Zhenwei Han, Shunli Kong, Jing Cheng, Hong Sui, Xingang Li, Zisheng Zhang, and Lin He, *Industrial & Engineering Chemistry Research,* **58**, Iss. 32: 14785 (2019); https://pubs.acs.org/doi/abs/10.1021/acs.iecr.9b02143
7. Qianyu Wang, Emmanuel Oluwaseyi Fagbohun, Houkun Zhu, Abid Hussain, Fang Wang, and Yanbin Cui, *Separation and Purification Technology*, **321**: 124205 (2023); https://doi.org/10.1016/j.seppur.2023.124205
8. Oxana V. Gorbunova, Olga N. Baklanova, Tatiana I. Gulyaeva, Anastasia V. Vasilevich, Alexey B. Arbuzov, Mikhail V. Trenikhin, and Alexander V. Lavrenov, *Adsorption*, **30**: 663 (2024); https://doi.org/10.1007/s10450-024-00467-6
9. K. Maheshwari, M. Agrawal, and A. B. Gupta, *Novel Materials for Dye-Containing Wastewater Treatment*, **1**: 25 (2021); https://doi.org/10.1007/978-981-16-2892-4_1
10. N. Puvaneswari, J. Muthukrishnan, and P. Gunasekaran, *Toxicity Assessment and Microbial Degradation of Azo Dyes* (2006), p. 618–626; http://nopr.niscpr.res.in/handle/123456789/6554
11. Mahmood M. Saleh, Hamadi Khemakhem, Ismel K. Jassim, and Raed Hashim Al-Saqa, *Ochrona przed Korozją*, **23,** No. 5: 543 (2024); doi:10.15199/40.2024.1.2
12. Abdullah M. Ali, Raed Alsaqa, and Nashwa Salhuddin Sultan, *International Journal of Thermodynamics*, **25**, Iss. 2: 33 (2022); https://doi.org/10.5541/ijot.1003950
13. Ilze Oshina and Janis Spigulis, *Journal of Biomedical Optics*, **26**, Iss. 10: 100901 (2021); https://doi.org/10.1117/1.JBO.26.10.100901
14. Veselinka Grudic, Ivana Boskovic, Dragan Radonjic, Zeljko Jacimovic, and Bojana Knezevic, *Iranian Journal of Chemistry and Chemical Engineering*, **38**, Iss. 2: 127 (2019); doi:10.30492/ijcce.2019.30659
15. Tao Chen, Tianxing Da, and Yan Ma, *Journal of Molecular Liquids*, **322**: 114980 (2021); https://doi.org/10.1016/j.molliq.2020.114980
16. Xueyong Zhou and Xin Zhou, *Chemical Engineering Communications*, **201**, Iss. 11: 1459 (2014); https://doi.org/10.1080/00986445.2013.818541
17. Muhammad N. Al-Fiydh, Hawraa F. Najm, Faiq F. Karam, and Sadiq J. Baqir, *Results in Chemistry*, **10**: 101680 (2024); https://doi.org/10.1016/j.rechem.2024.101680
18. T. G. Korotkova, A. M. Zakolyukina, and S. A. Bushumov, *Russian Journal of Physical Chemistry A*, **98**, Iss. 8: 1838 (2024); https://doi.org/10.1134/S0036024424700924
19. Ayhan Abdullah Ceyhan, Ömer Şahin, Orhan Baytar, and Cafer Saka, *Journal of Analytical and Applied Pyrolysis,* **104**: 378 (2013);

https://doi.org/10.1016/j.jaap.2013.06.009
20. Zhongbei Li, Ting Ren, Xiangchun Li, Ming Qiao, Xiaohan Yang, Lihai Tan, and Baisheng Nie, *International Journal of Mining Science and Technology*, **33**, Iss. 4: 389 (2023); https://doi.org/10.1016/j.ijmst.2022.12.006
21. Jizhen Zhang, Ken Aldren S. Usman, Mia Angela N. Judicpa, Dylan Hegh, Peter A. Lynch, and Joselito M. Razal, *Small Methods*, **7**, Iss. 8: 2201527 (2023); https://doi.org/10.1002/smtd.202201527
22. Marilyn E. Jacox and Dolphus E. Milligan, *The Journal of Chemical Physics*, **53**, Iss. 7: 2688 (1970); https://doi.org/10.1063/1.1674392
23. S. Alfadhli, A. A. A. Darwish, S. Soliman, E. F. M. El-Zaidia, I. S. Yahia, Farah Laariedh, Ahmed Alatawi, A. Bahamran, Nada M. Alatawi, and Taymour A. Hamdalla, *Journal of Non-Crystalline Solids*, **601**: 122044 (2023); https://doi.org/10.1016/j.jnoncrysol.2022.122044
24. Orlando F. Cruz Jr., Jarosław Serafin, Fatima-Zahra Azar, Mirian E. Casco, Joaquín Silvestre-Albero, Dachamir Hotza, and Carlos R. Rambo, *Fuel*, **358**, Pt. B: 130329 (2024); https://doi.org/10.1016/j.fuel.2023.130329
25. Jeffrey C. Nankervis and Robert B. Furlong, *Fuel*, **59**, Iss. 6: 425 (1980); https://doi.org/10.1016/0016-2361(80)90196-9
26. Eszter Rápy and Szende Tonk, *Molecules*, **26**, No. 17: 5419 (2021); https://doi.org/10.3390/molecules26175419
27. Małgorzata Wasilewska, Adam Wojciech Marczewski, Anna Deryło-Marczewska, and Dariusz Sternik, *Journal of Environmental Chemical Engineering*, **9**, Iss. 4: 105459 (2021); https://doi.org/10.1016/j.jece.2021.105459
28. Imelda Guerrero-Coronilla, Liliana Morales-Barrera, and Eliseo Cristiani-Urbina, *Journal of Environmental Management*, **152**: 99 (2015); https://doi.org/10.1016/j.jenvman.2015.01.026
29. Ana Carolina Ferreira Piazzi Fuhr, Cristiane Ferraz de Azevedo, Naushad Ahmad, Sonaimuthu Mohandoss, Guilherme Luiz Dotto, and Fernando Machado Machado, *Journal of Molecular Liquids*, **407**: 125191 (2024); https://doi.org/10.1016/j.molliq.2024.125191
30. Qingli Chen, Jie Liao, Sihua Zeng, and Li Zhou, *Materials*, **17**, Iss. 10: 2391 (2024); https://doi.org/10.3390/ma17102391
31. Nur Aimi Jani, Larbi Haddad, Ahmed Saud Abdulhameed, Ali H. Jawad, Zeid A. ALOthman, and Zaher Mundher Yaseen, *Biomass Conversion and Biorefinery*, **14**: 12441 (2024); https://doi.org/10.1007/s13399-022-03319-x
32. Robert A. Latour, *Journal of Biomedical Materials Research Part A*, **103**, Iss. 3: 949 (2015); https://doi.org/10.1002/jbm.a.35235
33. Mohini Singh, Mohd. Rayaz, and R. Arti, *Environmental Progress & Sustainable Energy*, **43**, Iss. 1: e14259 (2024); https://doi.org/10.1002/ep.14259